Numerical–Experimental Benchmarking of a Probabilistic Code for Prediction of Voltage Holding in High Vacuum

N. Pilan, A. Kojima, R. Nishikiori, M. Ichikawa, J. Hiratsuka, R. Specogna, A. De Lorenzi, M. Bernardi, L. Lotto, P. Bettini, and M. Kashiwagi

***Abstract*— In the framework of the program for the construction of 1 MeV–16 MW negative neutral beam injector (NNBI) for ITER, a research and development activity on voltage holding in vacuum has been initiated since 2009, aimed at supporting the design, construction, and development of the NNBI accelerator. For this purpose, the voltage holding prediction model (VHPM) previously developed has been updated. In the VHPM, the effect of the anodic electric field and the cathodic electric field on the probability of breakdown is evaluated by means of two exponents: α and γ. On the basis of the experimental results from different test stands and of detailed 3-D numerical simulation of the corresponding electric-field configurations, the predictions of the VHPM numerical code have been benchmarked. New exponents, α and γ, have been proposed to obtain a more precise location of the weak point of the system and a better prediction of the maximum withstanding dc voltage in high vacuum.**

***Index Terms*— High voltage (HV), neutral beam injection, vacuum.**

I. Introduction

THE design of the multistage electrostatic accelerator for the ITER negative neutral beam injector (NNBI) [2] based on a standard approach, which assumes the electric field at the electrodes as design parameter, is far from being sufficient to comply with the voltage holding requirements. For this reason, a research activity has started, aimed at developing a generalized criterion for voltage holding in a multielectrode–multivoltage dc system insulated by large vacuum gaps [3]. This criterion is intended to apply to any system with any electrodes' shape, different dc voltages, and a background gas pressure located at the far left-hand side of the Paschen curve.

Manuscript received June 7, 2017; revised October 6, 2017; accepted November 15, 2017. Date of publication December 11, 2017; date of current version May 8, 2018. This work was supported by Fusion for Energy. The review of this paper was arranged by Senior Editor E. Surrey. *(Corresponding author: N. Pilan.)*

N. Pilan, A. De Lorenzi, M. Bernardi, and L. Lotto are with the Consorzio RFX, EURATOM-ENEA Association, Padua, Italy (e-mail: nicola.pilan@igi.cnr.it).

A. Kojima, R. Nishikiori, M. Ichikawa, J. Hiratsuka, and M. Kashiwagi are with the NB Tech. Heating Group, Naka fusion Institute QST, Naka, Japan.

R. Specogna is with the Dipartimento Politecnico di Ingegneria e Architettura, Università di Udine, Udine, Italy.

P. Bettini is with the Consorzio RFX, EURATOM-ENEA Association, Padua, Italy, and also with the Dipartimento di Ingegneria Industriale, Università di Padova, Padua, Italy.

Color versions of one or more of the figures in this paper are available online at http://ieeexplore.ieee.org.

Digital Object Identifier 10.1109/TPS.2017.2775246

So far, a precise initiation mechanism of the breakdown in vacuum for the long gap cases ($d > 5$–10 mm) has not been identified yet. In this case, thermal instabilities due to Fowler–Nordheim (FN) electron emission from the cathode would require an enhancement geometric factor β of the electric field greatly higher than the amplification factor expected considering the dimension of the surface roughness observed by SEM techniques [4] leading many authors to consider the FN emission from dielectric inclusions at the cathode [5] as additional mechanism to extract electrons by macroscopic electric field in the MV/m range; nevertheless, the FN electron emission does not consider for the total voltage effect (TVE) [3], which is the nonlinearity of the breakdown voltage with the gap length d: $V \propto d^c$ ($c < 1$). The TVE could be explained by the microparticle theory (clump) [6], [9], and the weak point of this theory concerns the regeneration of such particles. Once a device has been conditioned, no degradation of the voltage holding should occur if the electrodes are kept in high vacuum; the reality does not confirm this expectation, although high electric fields, in dc voltages, can modify the electrode surface [7], and microparticles could be generated by FN thermal instabilities, which weaken an existing protrusion enough to allow it to elongate and eventually a "clump" to break off from the surface. Other theories applicable at shorter gaps are: secondary electron emission mechanism and charge trapping/detrapping at localized sites [5], while theories like the electron avalanche induced by soft X-ray emission produced by secondary electrons at the anode [8] applicable also to the longer gaps have so far neither experimental evidence, nor a quantitative formulation for a direct comparison with the experiment.

In 2010, an innovative tool for the determination of the breakdown voltage in an electrostatic system of any complexity has been proposed: the voltage holding prediction model (VHPM) [1] based on the following experimental evidences:

1) the existence of the TVE;
2) the probabilistic nature of the breakdown occurrence;
3) the electrodes area effect on the breakdown voltage (the larger the area, the lower the breakdown voltage);
4) the polarity effect (inverting the polarity for an electrostatic system with all the electrodes in the same condition—material and treatment—the lowest breakdown voltage occurs when negative polarity is

applied to the electrode having the greater electric-field concentration).

The VHPM is applicable at the left-hand side of the Paschen curve (i.e., background gas pressure $p \leq 10^{-6}$ mbar). The VHPM is based on the Cranberg/Slivkov breakdown criterion [9] for the breakdown occurrence, described by the inequality

$$W = E_K \cdot E_A^{2/3} \cdot U > W_L \tag{1}$$

where W_L is a parameter depending on the electrodes material properties, U is the applied Voltage, E_K is the electric field at the cathode point from which the clump starts its trajectory, and E_A is the electric field at the position at the anode side, where the clump clashes. The VHPM includes the Slivkov's criterion inside a probabilistic frame. The surface density of critical clumps (i.e.,) clumps for which (1) is satisfied and N [m^{-2}] is expressed as an increasing function of W

$$N(W) = \left(\frac{W}{W_0}\right)^m. \tag{2}$$

Integrating all contributes along all the cathodic surfaces, it can be shown that [1] the overall breakdown probability is

$$P = 1 - \exp\left[-\int \left(\frac{W}{W_0}\right)^m \cdot dA\right] \tag{3}$$

where W can be defined as "breakdown variable." To evaluate W, VHPM calculates the trajectory of the clump in order to identify the local electric field E_A at the impact point. The quantity W_0 is the value of W necessary to have a breakdown probability equal to 63.2% in a couple of ideal plane-parallel electrodes having a surface of 1 m^2. In [13], it has been demonstrated that another basic breakdown mechanism (e.g., Latham's photoelectric cascade [8]) can lead to the general formulation of the breakdown variable

$$W = E_K^{\gamma} \cdot E_A^{\alpha} \cdot U. \tag{4}$$

Several tests carried out in the past years using stainless steel electrodes, with gap length from 10 to 100 mm and with classical plane–plane and sphere–plane geometries, have shown a fairly good agreement with VHPM, using the W formulation given in (1) [9].

Recently, the VHPM has been applied to the full-scale prototype of the high-voltage bushing (HVB) SF_6-vacuum for the ITER NBI injector (1-MV max. voltage; a multielectrode system, with the longest gap of 1300 mm to sustain 1 MV); this model has been benchmarked against the results of an HV test campaign carried out at the QST laboratories aimed at reaching the full voltage holding capability of the system. In this case, the model predictions have shown some inconsistencies with the measurements. A possible explanation has been envisaged in the inappropriate values of the exponents α and γ (from Cranberg–Slivkov model). This paper presents the results obtained with different values of α and γ (obtained with a particular fitting procedure hereinafter described and discussed).

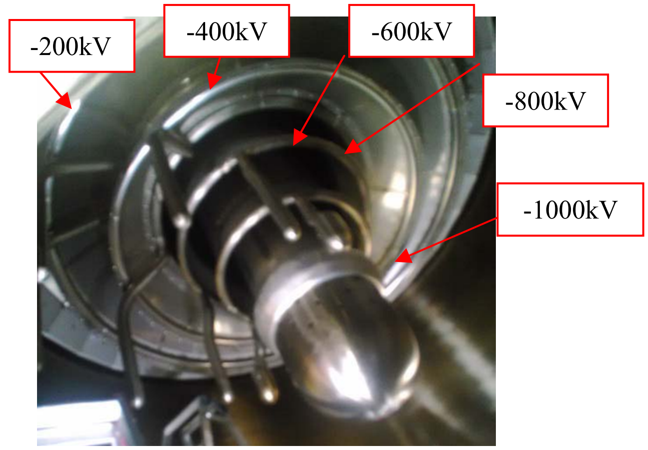

Fig. 1. Bushing electrodes in high vacuum.

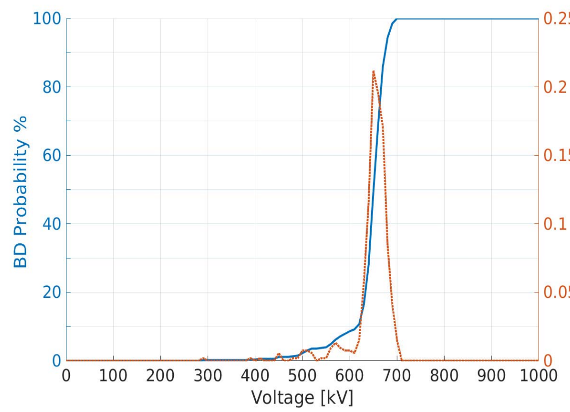

Fig. 2. Experimental results. Blue: cumulative breakdown probability. Red: breakdown voltage distribution.

II. Experimental Setup and Results of the HV Tests

A. Setup Description

The system is a multistage HV dc feedthrough, which separates pressurized SF_6 from the NBI vacuum; the bushing is rated at −1 MV dc and it is composed by five stages, 200-kV dc each. The HVB is described in [10, Sec. 4]. This contribution is focused only on the voltage holding issues concerning vacuum, which is the most critical issue, as discussed in [12].

The HVB is inserted in a cylindrical vacuum vessel (3 m in diameter and 3.1 m high) [11]. A picture of the coaxial stainless steel electrodes in vacuum is shown in Fig. 1. Four pairs of cooling pipes protrude inside the vacuum chamber as cantilever beams from the coaxial electrodes which they are connected to. The pipes and the bottom part of the −1 MV conductor have been terminated by spherical screens in order to avoid electric-field concentrations. The voltage was applied by a Cockcroft–Walton, negative polarity power supply and it was applied to all the stages by a voltage divider (no resistors were adopted to limit the breakdown currents). The pressure of the vacuum vessel was in the order of 10^{-7} mbar.

The experimental results are shown in Fig. 2 considering the distribution of the breakdown voltages during the HV test and

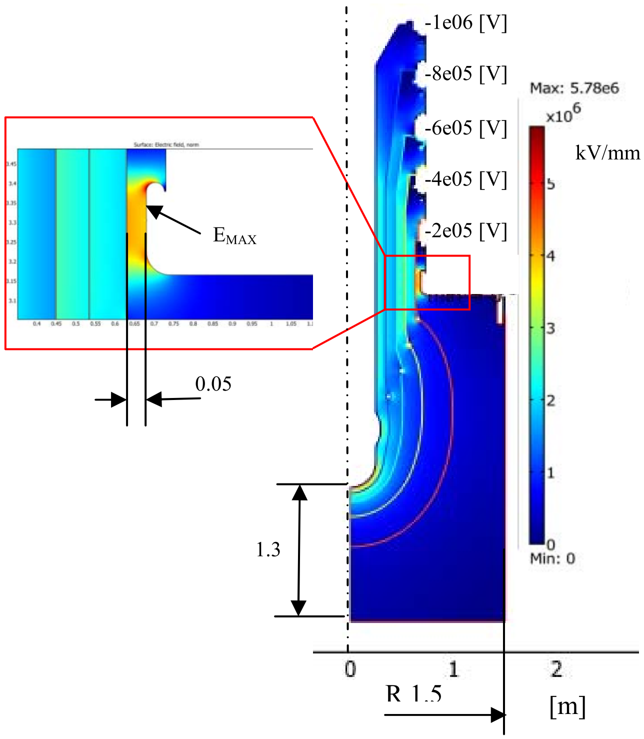

Fig. 3. Electrostatic field map at nominal voltages. Results of the 2-D axial symmetric finite element (FE) model.

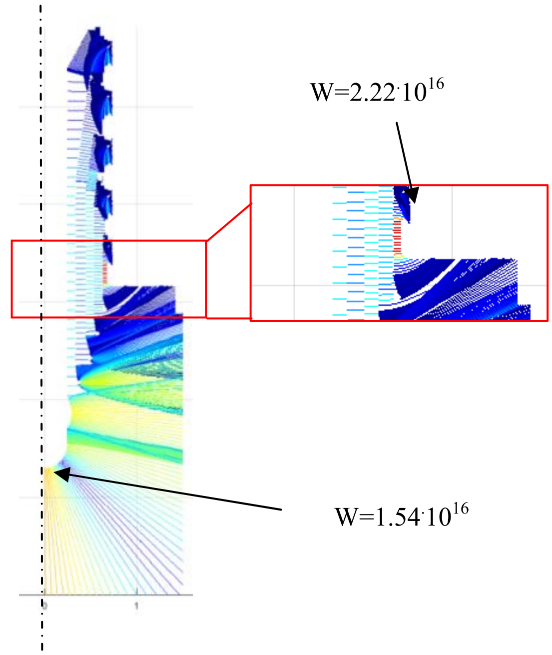

Fig. 4. Trajectories of negative-charged particles. Color scale according to the magnitude of $W = E_a^{2/3} \cdot E_c \cdot U$.

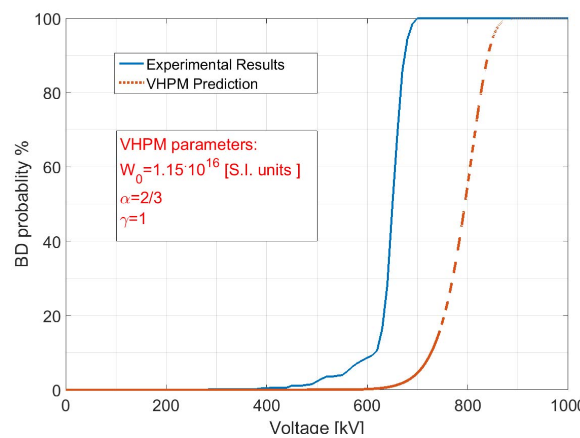

Fig. 5. Breakdown probability versus maximum voltage, comparison between experimental results and VHPM prediction. The intermediate stage voltages are distributed according to the following fractions (4/5, 3/5, 2/5, 1/5) of the maximum voltage.

the cumulative breakdown probability associated with such experimental data.

The maximum withstanding voltage was 705 kV after 75 h of HV conditioning in high vacuum.

Additional tests were carried out applying voltage individually at each stage while the other stages were at the ground potential, and during these tests, it has been possible to sustain easily up to 240 kV in each configuration.

B. Electric-Field Calculations

The 2-D electrostatic field map at the nominal voltages (-1000 kV, -800 kV, ..., 0 kV) in vacuum is shown in Fig. 3. The highest calculated electric field is between the -200 kV coaxial screen and the ground potential: the electric field at the cathode side on the screen is 3.43 kV/mm while the correspondent electric field at the anode side is 5.80 kV/mm. The electric field on the symmetry axis is 4.48 kV/mm on the bottom surface of the screen, at 1-MV stage, on the cathode side, while it is 0.20 kV/mm at the anode side on the grounded vessel.

III. First Benchmark Between Numerical Code and Experimental Results

The calculation of the breakdown probability has been done according to (3) and the procedure described in [13]. The physical quantity considered for the discharge initiation is W, as defined in (4). If $\gamma = 1$ and $\alpha = 2/3$, we obtain Slivkov's formulation [9]. Two Weibull parameters, m and W_0, characterize the electrode materials and the surface treatments (e.g., finishing and cleaning procedure) in (3). The knowledge of these parameters is necessary to use the code as a predictive tool. The first benchmark between experimental results and numerical prediction has been done by adopting Slivkov's exponents $\gamma = 1$ and $\alpha = 2/3$, with $W_0 = 1.1 \cdot 10^{16}$ [SI units] and $m = 8$, as reported in [1]. The results of the numerical analyses are shown in Fig. 4: the warmer the color, the higher the W parameter and the higher is the breakdown probability. The weakest point shown in Fig. 4 is located between the 200-kV stage and the grounded vessel, where the maximum $W = 2.2 \; 10^{16}$ [SI units] is achieved. The second-weakest point is shown in Fig. 4 by the trajectory along the symmetry axis, between the -1 MV screen and the grounded vessel, with $W = 1.54 \; 10^{16}$ [SI units]. As a matter of fact, this is the point, where the totality of the breakdown occurred.

Fig. 5 shows the prediction of the breakdown probability curve for the whole bushing. The comparison with the

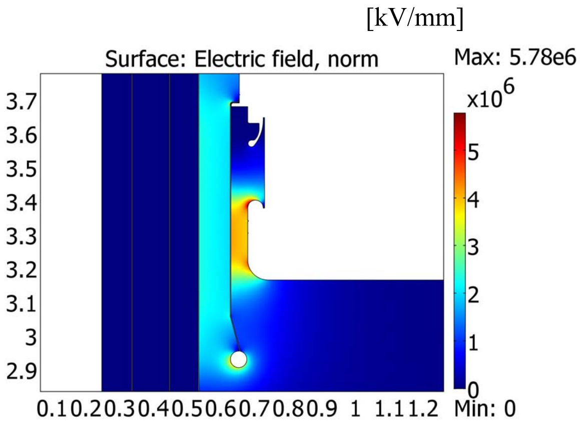

Fig. 6. Electrostatic field map polarizing only on the last accelerating stage at -200 kV_{dc}.

measured breakdown voltage distribution shows a prediction in excess in the order of 30%. Instead, the experimental observation that the breakdown occurs in a location where the breakdown probability should be lower than where predicted requires a detailed analysis, hereinafter discussed.

The experimental results have also shown that each single stage sustained easily voltages up to 240-kV dc; so the VHPM has been run to calculate the breakdown probability only for the last accelerating stage (the stage between -200 kV conductor and the grounded potential). The electric-field distribution for this new case, called "Single Stage," is shown in Fig. 6. The electric-field map is almost equal to the one shown in Fig. 3 for the region between the -200 kV and the ground potential, while it has a reverse direction in the region between the -200 and the -400 kV screen; the electric field is equal to zero in all the other regions. The breakdown probability associated with Fig. 6 has been then calculated. The results of these analyses are shown in Fig. 7.

It is interesting to observe that the model predicts a breakdown probability relatively low if compared with the experimental results of the single stage, and the model predicts a 60% breakdown probability with a voltage $U = 160$ kV_{dc}, but the experimental evidence shows that each single stage has been conditioned up to 240 kV_{dc} rapidly.

Instead, the whole multistage system has been conditioned in high vacuum up to 705 kV after 75 h of cumulative voltage time application, and during this test, the maximum voltage between two adjacent stages was $700/5 = 140$ kV. As pointed out in Section II, the weak point of the multistage test was the gap between the -1 MV screen and the grounded potential, along the axis of the bushing. The abscissa of the function reported in Fig. 7 has been multiplied by 5 and the results have been compared in Fig. 8 with the dotted line plot of Fig. 5. The two plots overlap each other, meaning that the contribution of all other stages, different from the 200-kV stage, is negligible.

Therefore, there is a clear inconsistency between the model prediction and the experimental results for the present multistage system, which includes both short and long vacuum gaps at the same time.

The inconsistency is related to the definition of W in the VHPM. In fact, it is interesting to observe that Slivkov's

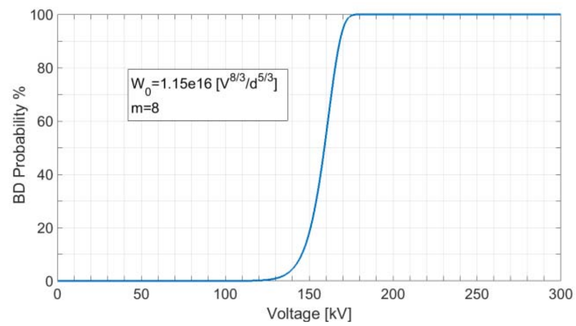

Fig. 7. Breakdown probability versus applied voltage. The voltage has been applied only to the -200 kV stage and kept to zero in the other stages. $W_0 = 1.15\ 10^{16}$, $m = 8$, $\alpha = 2/3$, and $\gamma = 1$.

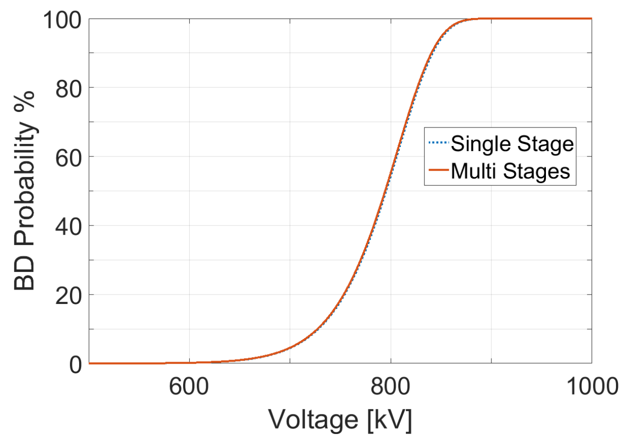

Fig. 8. Comparison of breakdown probabilities between the "Multistage" case (solid red) and the "Single Stage" (with the voltages amplified by a factor 5, blue dotted line). $W_0 = 1.1 \cdot 10^{16}$, $m = 8$, $\alpha = 2/3$, and $\gamma = 1$. The Single Stage plot is slightly on the right of the Multistage plot. At BD Probability = 50%, a difference of 2 kV exists between the two cases.

formulation of W gives to the electric field at the anode side an exponent $\alpha = 2/3$, which is lower than γ, according to the experimental observation on the polarity effect [9]; nevertheless, Slivkov's triple product requires a relatively high electric field also at the anode side to initiate the breakdown. In the case of the HVB, we know that the insulation is characterized by a weak point along the bushing's axis. As a matter of fact, a strong electric field is applied at the cathode side (3.15 kV/mm at -705 kV), where the maximum voltage drop is located, whereas a relatively low electric field (0.14 kV/mm at -705 kV) is applied at the anode side. This is the reason why we have proposed to modify α and γ with respect to the values, which would come from Slivkov's theory.

IV. Derivation of New Exponents of VHPM

The modification of the α and γ exponents has been implemented by fitting the results of several experimental campaigns carried out in different configurations with stainless steel electrodes.

A set of experimental results in terms of maximum voltage and electric field at anode and cathode sides have been collected and analyzed. The maximum voltage obtained experimentally can be thought as the superposition of two types of

TABLE I
EXPERIMENTAL RESULTS

i#	Lab.	Gap *[mm]*	E_k *[kV/mm]*	E_A *[kV/mm]*	U *[kV]*	Ref.	W [S.I.]
1	HVPTF	30	26.6	9.5	410		3.4e08
2	HVPTF	30	10.7	30	450		3.2e08
3	HVPTF	15	32.7	17.3	320		3.0e08
4	HVPTF	10	26.9	17	199	[13]	1.8e08
5	HVPTF	10	18.1	28.6	212	[13]	1.8e08
6	HVPTF	10	23	23	230	[13]	2.0e08
7	CERN	90	6	6	540	[16]	2.7e08
8	CERN	50	8	8	400	[16]	2.3e08
9	CERN	70	7	7	490	[16]	2.7e08
10	CERN	30	9.3	9.3	280	[16]	1.7e08
11	CERN	10	14.5	14.5	145	[16]	1.1e08
12	QST	1290	3.1	0.14	705	[11]	2.0e08

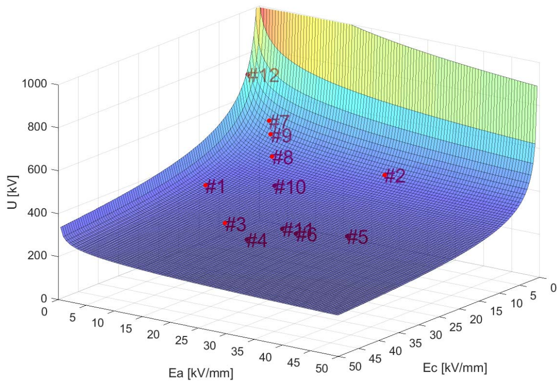

Fig. 9. Least square fit of the results reported in Table I. The red numbers are assigned according to the first column of Table I.

statistic distributions. The first type of voltage distribution can be associated with a specific configuration under test. Once a device has been conditioned, the maximum withstanding voltage is not always at the same value after the occurrence of a breakdown. The second type of breakdown voltage distribution concerns experiments that are nominally identical; if we compare the maximum voltage of two experiments that have the same electrode geometry, material and surface treatment, we are comparing two different distributions of voltages. It is expected that conditioning procedure and external circuit characteristics, which determine the energy dissipated during each breakdown, have also an influence on the voltage holding of the system [14]; typically these two causes have effects, which enlarge the breakdown voltage spread in a statistical manner.

The derivation of W_0 and m of (3) should be done considering the results of a relatively high number of experiments, which are nominally identical, a requirement very hard to achieve in practice, since the conditioning of a single test typically can last several hours.

In general, during our experimental campaigns, we can provide information about the first type of voltage distribution having lower scattered data than the second type. In VHPM, such information is related to the values assumed by the parameter m (the higher m is, the lower is the dispersion of the breakdown voltages). It is interesting to observe that if m tends to infinity, the probabilistic model becomes deterministic and the electrode area no longer has effect. In order to benchmark only the coefficients α and γ with the experimental results, a list of maximum breakdown voltages and corresponding electric fields have been prepared considering the experimental results obtained in our laboratory (HVPTF [15]), at the QST laboratories and in literature [16]. The experimental data, reported in Table I, concern stainless steel electrodes with a surface roughness Ra < 3.2 μm. No information about the voltage distribution is provided.

Let us assume that all the experimental data of Table I correspond to same triple product W_L, which represents a situation of incipient discharge. According to this hypothesis, (4) can be applied to the ith ($i = 1, \ldots, 12$) experimental data of Table I, as shown in

$$W_L = U_i \cdot E_{ik}^{\gamma} \cdot E_{iA}^{\alpha} \tag{5}$$

Substituting in (5) the following expressions: $x_i = \log(E_{ik})$, $y_i = \log(E_{iA})$, $z_i = \log(U_i)$, and $\zeta = \log(W_L)$, it is possible to derive (6), which represents a plane in the 3-D space described by the coordinates x, y, and z:

$$\zeta = z_i + \gamma \cdot x_i + \alpha \cdot y_i. \tag{6}$$

The coefficients α and γ can be obtained by fitting the experimental results of Table I by a last square method solving for a 3×3 linear system. The results of the fit are: $\alpha = 0.10$, $\gamma = 0.29$, and $W_L = 1.98 \cdot 10^8$ (S.I. units). Fig. 9 shows the best fit surface in the space Ec, Ea, and U.

The last column in Table I reports the value of W associated with each experimental point according to the new exponents. Although a not negligible spread exists in terms of W, it is necessary to highlight that the correspondent spread in the voltage prediction is relatively limited being $U \propto W_L^{((\alpha+\gamma)/(\alpha+\gamma+1))} = W_L^{0.7}$ and $W_L > 1$.

V. New Benchmark Between Numerical Code and Experimental Results

The analyses on the HVB described in Section II have been repeated considering the new exponents $\alpha = 0.10$ and $\gamma = 0.29$ and assuming a relatively high $m = 25$, as reported in [13]. If m is high ($>10 \div 15$), the numerical model tends to a deterministic approach, where the discharge is initiated exactly in the position having the maximum W. Under this hypothesis, the substitution $W_0 = W_L$ is allowed. The results of this new benchmark are shown in Fig. 10, where the particles' trajectories are colored as usual according with the magnitude of W.

Again, the new probability curve, shown in Fig. 11, predicts breakdown voltages 30% larger than the experimental results (as found in Fig. 6), but the most critical region, as shown in in Fig. 10, is now along the bushing's axis as experimentally observed.

This improvement depends on the new exponents α and γ, which give more importance to the total voltage effect rather than the sole electric field contribute. For the sake of clarity, if we consider an ideal case having plane parallel electrodes, with $m \to +\infty$, the model predicts a breakdown voltage U

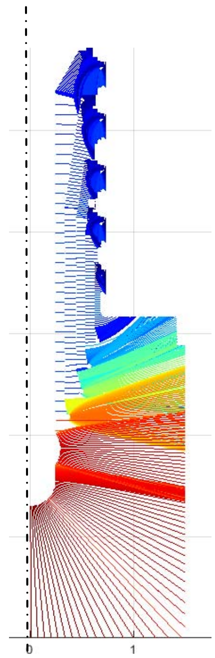

Fig. 10. Trajectories of negative-charged particles. The trajectories are colored according to the magnitude of $W = (\mathrm{Ea}^\wedge\alpha)^*(\mathrm{Ek}^\wedge\gamma)^*U$.

as only a function of the gap length d, as shown in

$$U \propto d^{\left(\frac{\alpha+\gamma}{\alpha+\gamma+1}\right)}. \tag{7}$$

In case of the former (Slivkov's) coefficients, the voltage resulted $U \propto d^{0.625}$ while in this new formulation it is $U \propto d^{0.286}$ with a pronounced voltage saturation effect in the long-gap region.

It must be pointed out that the HVB is a multielectrode–multivoltage system having two extreme situations: high electric fields in the region highlighted in Fig. 6, which has a relatively low voltage (i.e., short gap), and a region having very long gap and HV along the axis of the system.

The overestimation of the voltage breakdown is substantially due to the fact the number of "short-gap cases" in Table I is predominant; on the other hand, it is of great interest that—after the determination of α and γ exponents and W_L fitting experimental data—the VHPM now predicts correctly the position of the breakdown.

VI. Comparison Between 3-D and 2-D FE Models

The HVB described in Section II-A has a 2-D axial symmetric geometry, except for the presence of some cooling pipes breaking symmetry. A 3-D electrostatic model of the HVB with the cooling pipe detail has been developed to evaluate the effect of such detail in the evaluation of the breakdown probability.

Fig. 12 shows the electric-field distribution on the electrodes energized at nominal voltage. The maximum electric field on the bottom part of the sphere at 1 MV is 4.3 kV/mm, very close to the value determined by the 2-D model. The maximum electric field on the cooling pipe surfaces is 7 kV/mm on the −800 kV stage. Such a detail is obviously not present in the 2-D axial symmetric map shown in Fig. 3.

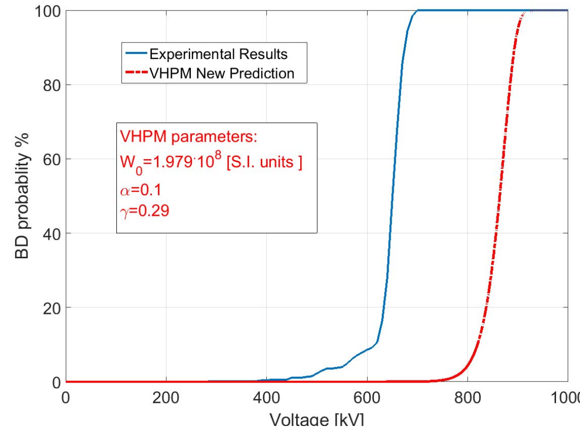

Fig. 11. Breakdown probability versus maximum voltage, comparison between experimental results and new VHPM prediction.

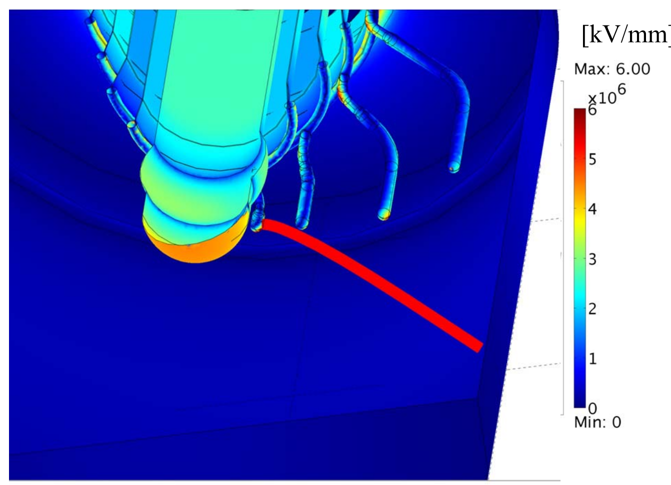

Fig. 12. 3-D FE analyses: electrostatic field map at nominal voltages.

A 3-D version of VHPM is not available yet, but it is presently under development. A preliminary calculation of some particle trajectories has been done on the basis of the 3-D electrostatic map of the model shown in Fig. 12.

The estimation of the maximum W parameter for the 800-kV cooling pipes has been done considering only the trajectory shown in Fig. 12 by red color passing through the point having the maximum electric field $\mathrm{Ek}_{800\,\mathrm{kV}} = 7$ kV/mm at the cathode, the corresponding point at the anode side has an electric field $\mathrm{Ea}_{800\,\mathrm{kV}} = 0.3$ kV/mm, and for such trajectory, it is possible to evaluate $W_{800\,\mathrm{kV}} = 2.8\mathrm{e}08$ [S.I.] by using the new exponents α and γ; on the other hand, the point on the bottom part of the sphere has $\mathrm{Ek}_{1\,\mathrm{MV}} = 4.6$ kV/mm, $\mathrm{Ea}_{1\,\mathrm{MV}} = 0.2$ kV/mm, and the full voltage (1 MV) the corresponding value of W is $W_{1\,\mathrm{MV}} = 3.0\mathrm{e}08$ [S.I.], which is greater than $W_{800\,\mathrm{kV}}$ and closer to the value obtained by using the 2-D model. This comparison partially confirms the reliability of the results obtained by the 2-D model described in the previous sections for the present geometry, which is not exactly axial-symmetric. Nevertheless, more detailed analyses will be carried out being the 3-D version of the VHPM necessary to simulate the real geometry of the electrostatic accelerator of the ITER NBI.

VII. Conclusion

A benchmark between experimental results and the numerical code has led to the definition of new exponents: α and γ. A more precise location of the weak point of the system and a better prediction of the maximum withstanding dc voltage in high vacuum has been verified; nevertheless, the validation process and the improvement of the probabilistic model still remain an ongoing activity that needs experimental data especially in the long vacuum gaps, whereas the TVE has a marked influence and the results in the published literature are limited.

Acknowledgment

This publication reflects the views only of the authors, and F4E cannot be held responsible for any use which may be made of the information contained therein. The views and opinions expressed herein do not necessarily reflect those of the ITER Organization.

References

[1] N. Pilan, P. Veltri, and A. De Lorenzi, "Voltage holding prediction in multi electrode-multi voltage systems insulated in vacuum," *IEEE Trans. Dielectr. Electr. Insul.*, vol. 18, no. 2, pp. 553–560, Apr. 2011.

[2] V. Toigo *et al.*, "A substantial step forward in the realization of the ITER HNB system: The ITER NBI test facility," *Fusion Eng. Design*, vol. 123, pp. 32–39, Nov. 2017.

[3] P. Spolaore, G. Bisoffi, F. Cervellera, R. Pengo, and F. Scarpa, "The large gap case for HV insulation in vacuum," *IEEE Trans. Dielectrics Electr. Insul.*, vol. 4, no. 4, pp. 389–393, Aug. 1997.

[4] R. V. Latham and E. Braun, "An investigation of pre-breakdown cathode microcratering," *J. Phys. D, Appl. Phys.*, vol. 3, no. 11, pp. 1663–1669, 1970.

[5] R. Latham, *High Voltage Vacuum Insulation: Basic Concepts and Technological Practice*. London, U.K.: Academic, 1995.

[6] L. Cranberg, "The initiation of electrical breakdown in vacuum," *J. Appl. Phys.*, vol. 23, p. 518, Jun. 1952.

[7] A. Descoeudres, Y. Levinsen, S. Calatroni, M. Taborelli, and W. Wuensch, "Investigation of the dc vacuum breakdown mechanism," *Phys. Rev. Accel. Beams*, vol. 12, p. 092001, Sep. 2009.

[8] R. V. Latham, *High Voltage Vacuum Insulation, New Perspective*. Bloomington, IN, USA: AuthorHouse, 2006.

[9] I. N. Slivkov, "Mechanism for electrical discharge in vacuum," *Soc. Phys. Technol. Phys.*, vol. 2, pp. 1928–1934, Sep. 1957.

[10] H. Tobari *et al.*, "DC ultrahigh voltage insulation technology for 1 MV power supply system for fusion application," *IEEE Trans. Plasma Sci.*, vol. 45, no. 1, pp. 162–169, Jan. 2017.

[11] A. Kojima *et al.*, "Achievement of 1 MV vacuum insulation with 5-stage electrostatic screens in high voltage bushing for ITER neutral beam injector," *Nucl. Fusion*, to be published.

[12] N. Pilan *et al.*, "A new deflection technique applied to an existing scheme of electrostatic accelerator for high energy neutral beam injection in fusion reactor devices," *Rev. Sci. Instrum.*, vol. 87, p. 02B325, Feb. 2016.

[13] A. De Lorenzi, N. Pilan, and E. Spada, "Progress in the validation of the voltage holding prediction model at the high-voltage padova test facility," *IEEE Trans. Plasma Sci.*, vol. 41, no. 8, pp. 2128–2134, Aug. 2013.

[14] K. Watanabe, M. Mizuno, and Y. Ohara, "DC voltage holding experiments of vacuum gap for high-energy ion sources," *J. Appl. Phys.*, vol. 72, no. 9, p. 3949, 1992.

[15] A. De Lorenzi, "HVPTF—The high voltage laboratory for the ITER Neutral Beam test facility," *Fusion Eng. Design*, vol. 86, nos. 6–8, pp. 742–745, Oct. 2011.

[16] F. Rohrbach, "Isolation sous vide," Tech. Rep. CERN 71-5, Jan. 1971.

[17] P. Bettini *et al.*, "Goal-oriented adaptivity in complementary geometric formulations for electrostatics," presented at the 21st Int. Conf. Comput. Electromagn. Fields, Daejeon, South Korea, Jun. 2017.

Authors' photographs and biographies not available at the time of publication.